Russian Geology and Geophysics © 2019, V.S. Sobolev IGM, Siberian Branch of the RAS
Vol. 60, No. 4, pp. 435–446, 2019 *DOI:10.15372/RGG2019042* *Geologiya i Geofizika*

Zirconology of the Lherzolite Block of the Nurali Massif (South Urals)[1]

A.A. Krasnobaev[a], A.I. Rusin[a], P.M. Valizer[b,✉], I.I. Likhanov[c]

[a] *Zavaritskii Institute of Geology and Geochemistry, Ural Branch, Russian Academy of Sciences, per. Pochtovyi 7, Yekaterinburg, 620075, Russia*

[b] *Ilmeny State Reserve, Miass, 456317, Russia*

[c] *V.S. Sobolev Institute of Geology and Mineralogy, Siberian Branch, Russian Academy of Sciences, pr. Akademika Koptyuga 3, Novosibirsk, 630090, Russia*

Received 30 October 2017; accepted 15 June 2018

Abstract—Data on the mineralogy, geochemistry, and geochronology of zircons from plagioclase and spinel lherzolite and dunites of the Nurali massif are presented. The age of the main-type zircons from lherzolites (plagioclase ones, 446.2 ± 2.8 Ma, and spinel ones 433.3 ± 3.4 Ma) and dunites (443.8 ± 6.9 Ma) suggests their synchronous crystallization (T_{av} = 440 ± 5 Ma). The metamorphic age of zircons is 410–415 Ma. In addition to grains belonging to the main subset, the older grains with an age between 527 and 2045 Ma and newly formed metasomatic grains with an age of 380–385 Ma were found. The structure and REE patterns of most zircons from ultramafic rocks point to their magmatic origin, which is probably related to crystallization of a fluidized mantle melt.

Keywords: lherzolite, dunite, zircon, geochemistry, REE, Th and U, age, Nurali massif

INTRODUCTION

The Nurali massif (NM), which is a part of the mafic-ultramafic allochthon of the same name, is located in the Southern Urals, at the mouth of the Miass River. It is a lens-shaped body (20 × 3.5 km), composed of spinel and plagioclase lherzolite, harzburgite, and dunite, exhibiting complex relationships with each other. The NM is bordered by a layered dunite—wehrlite—clinopyroxenite slice to the east, and by a serpentinite mélange incorporating blocks of a differentiated gabbro-diorite intrusion to the west (Fig. 1). Although these structural relations between the main units are recognized by all researchers, their internal structure and timing of tectonic emplacement of the Nurali allochthon are still not fully resolved (Rudnik, 1965; Savelieva, 1987, 2011; Knipper et al., 2001; Fershtater, 2013; and others). The peridotite block is interpreted either as a representative of root-zone orogenic lherzolites (Fershtater and Bea, 1996; Fershtater, 2013), overlapped by a layered dunite—wehrlite—clinopyroxenite unit, up to 400 m thick, which, in turn, is overlain by a differentiated gabbro-diorite intrusion (Savelieva and Denisova, 1983; Savelieva, 1987, 2011; Pertsev et al, 1997; Knipper et al., 2001; and others) or as a typical example of lherzolite-type ophiolite complexes, which do not contain any block of orogenic lherzolites.

Geochronological isotope studies of the Nurali massifs are scarce. The Re–Os and Sm–Nd isotope systems of the harzburgites, dunites, wehrlites, chromites, and gabbros (Tessalina et al., 2007) indicate that the detachment of a mantle block and its emplacement in the subcontinental lithosphere occurred at 1249 ± 80 Ma. The Late Vendian age (578 ± 18 Ma, Sm–Nd isochron method) of the Nurali hyperbasites (Popov et al., 2008) is difficult to interpret, given their complex geological history. At best, such dates can be perceived as age indicators of metamorphism, which may represent a combination of all age characteristics of the original rocks and subsequent resetting of the isotopic systems, which itself is a very ephemeral event. The most reliable age of zircons from diorites, which are classified as differentiates of a gabbro magma, is 399 ± 2 Ma (Fershtater et al., 2000). This age is interpreted to date emplacement of the NM gabbro-diorite intrusion. We have to admit that the age data for the NM ultramafic rocks are still controversial (Dobretsov et al., 2019).

GOALS AND OBJECTIVES

The main goal is to give the mineralogical and geochemical characteristics of zircons from ultramafic rocks of the Nurali massif within the probable time limits of its evolution.

To achieve this goal, it is necessary to solve several specific problems: (1) to isolate zircons from ultramafic rocks and (2) to establish the causes of heterogeneity of zircon grains, the nature of different coexisting zones and the growth sequence of zircon grains using polished zircons. After these steps, it possible to select the data points for isotope analysis, taking into account the important evolutionary

[1] This work is published as a discussion paper.

✉ Corresponding author.
E-mail adress: valizer@ilmeny.ac.ru (P.M. Valizer)

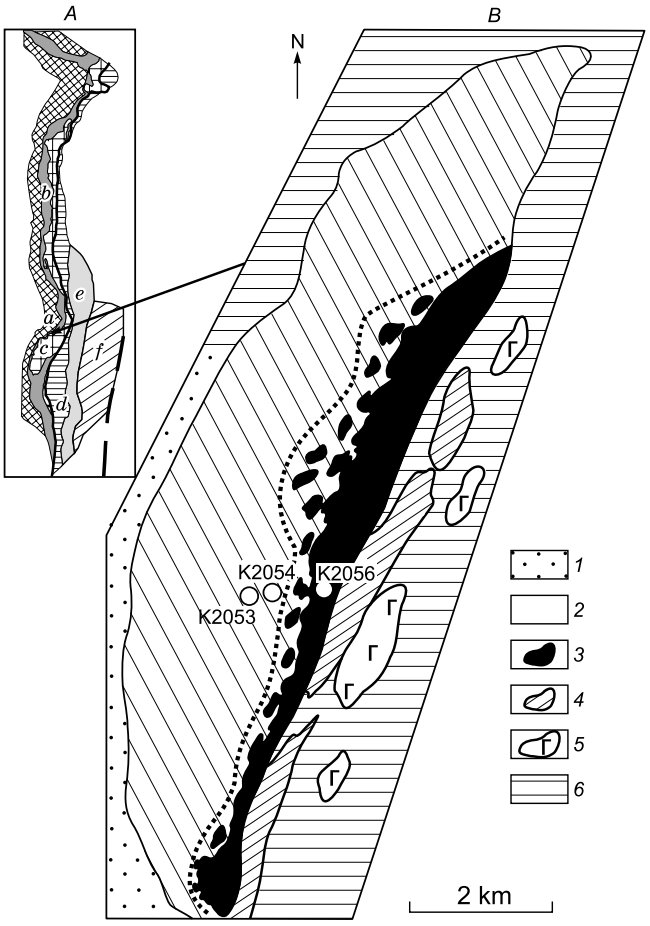

Fig. 1. The scheme of the structural zoning of the Urals (Puchkov, 2010) (*A*), schematic geological map of the Nurali massif (Rudnik, 1965; Savelieva, 1987; Fershtater, 2013) (*B*). *A*: *a*, Ural Foredeep; *b*, West Uralian Megazone; *c*, Central Uralian Megazone; *d*, Tagil–Magnitogorsk Zone; *e*, East Uralian Megazone; *f*, Trans-Uralian Megazone. *B*: *1*, Upper Proterozoic rocks (quartzites, mica schists); *2*, *3*, peridotite block (*2*, spinel and plagioclase lherzolites, *3*, dunites and harzburgites); *4*, dunite–wehrlite–clinopyroxene banded complex; *5*, gabbro, amphibolites, and diorites; *6*, serpentinite mélange. Samples K2053–K2054, plagioclase and spinel lherzolite, K2056, dunite.

stages of zircon grains and (3) to perform analysis, using only the SHRIMP technique, taking into account the established sequence of selected points.

METHODS

Samples of the NM ultramafic rocks were collected for analysis, based on the conclusions of Rudnik (1965), who provided a detailed description of their color variation and extent of weathering and serpentinization. Preference was given only to equigranular massive varieties.

Zircons isolated from spinel (Spl, K2054) and plagioclase (Pl, K2053) lherzolites from the central part, and dunites (Du, K2056) from the eastern part of the massif (Fig. 1) were used in this study. Whole-rock samples (150–200 kg) were crushed and pulverized to the –0.25 μm fraction, washed in tap water to remove magnetic and electromagnetic admixtures. The heavy-mineral residue (0.2–0.5 cm^3) was sorted by hands under the microscope. The polished zircons were analyzed by SHRIMP (Williams, 1998) for their U and Th contents and isotopic ratios. The REE content of zircons was determined by secondary ion mass spectrometry with a CAMECA IMS-4F ion microprobe. Samples were imaged for secondary electrons using a 25 μm spot. Measurements consisted of five repeated cycles of signal accumulation and varied depending on its intensity. Calibration was performed using appropriate reference standards (Fedotova et al., 2008). Measurements of REE were made on the same spots of zircon grains that were previously analyzed for U–Pb age.

RESULTS AND DISCUSSION

Morphology and internal structure of zircons. Lherzolite and dunite zircons have not been studied sufficiently and their descriptions in the literature are still limited to a few cases. Cathodoluminescence (CL), backscattered electron (BSE) and optical images of zircon grains are shown in Fig. 2. Lherzolites yielded a texturally complex population of zircon grains in terms of their shape, internal structure, transparency, and secondary transformations. This population is dominated by subhedral colorless zoned zircon grains whose textural characteristics suggest a magmatic origin. Among zircons from Spl (Fig. 2), there is a subset of grains (3, 4, 5, and 6) with textural evidence of brittle deformations and rehealing. Fractured zircon grains (1 and 9) have been transferred to the "new" state without disintegration into fragments and retained their original zoning structure. Such a transition occurs only under dry conditions close to the parameters of granulite-facies metamorphism. Also present are few zircon grains with a different origin, which show evidence of fracturing and dissolution (gr. 8), and replacement of early generation grains with a patchy (CL) structure (gr. 2), as well as early-generation translucent euhedral grains with original zoning and primary inclusions (gr. 7).

Zircons from Pl are largely of magmatic origin (gr. 1, 4, 5, 7, 8, etc.). They occur as rounded fragments (gr. 2, 3, and 6) with evidence of fracturing and dissolution (Fig. 2). Comparison shows that Spl zircons are typically more strongly altered than Pl zircons, taking into account the presence of deformed grains. A few old grains showing a varied degree of preservation (3, Pl, 8, Spl) and variable characteristics are not directly related to lherzolite, but their derivation from the mantle source is highly likely.

Many Du zircons are also comparable both structurally and texturally with the main type igneous grains from lherzolites. Based on the internal zoning pattern, grains 7 and 9 can be attributed to a different subset, and the presence of a large inclusion in grain 5 is consistent with growth during melting. Of particular importance for dunites are the pres-

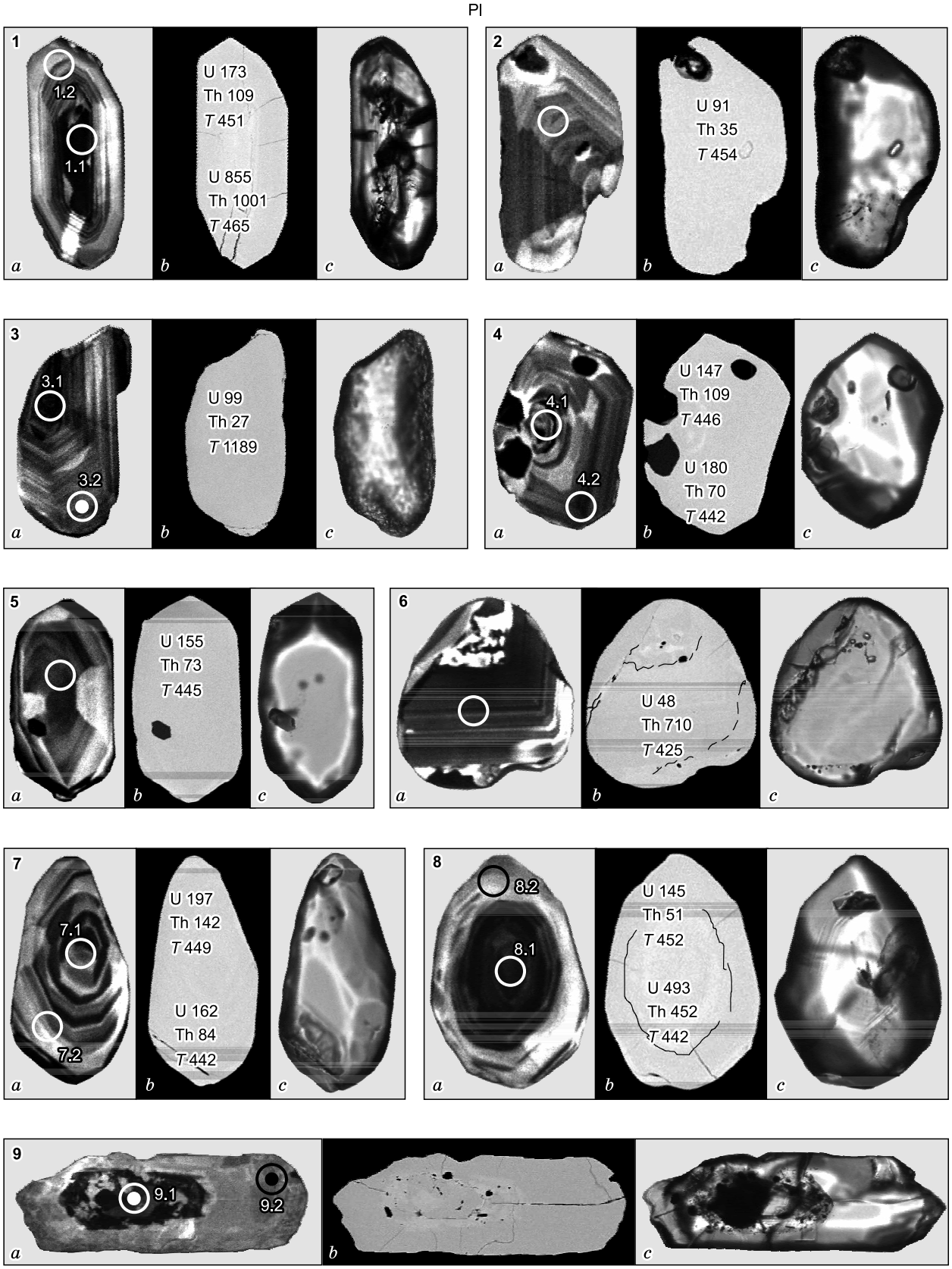

Fig. 2. Mineralogical, geochemical, and geochronological features of zircons from lherzolites (Pl, Spl) and dunites (Du) of the Nurali massif. Numerals show the numbers of grains and spots (Table 1), U and Th contents (ppm), $^{206}Pb/^{238}U$ age (*T,* Ma). *a*, CL; *b*, BSE; *c*, optical, transmitted light. In spots 4.2, 8.2, Spl and 3.2, 9.1–9.2 Pl, only REE analyses (Fig. 5).

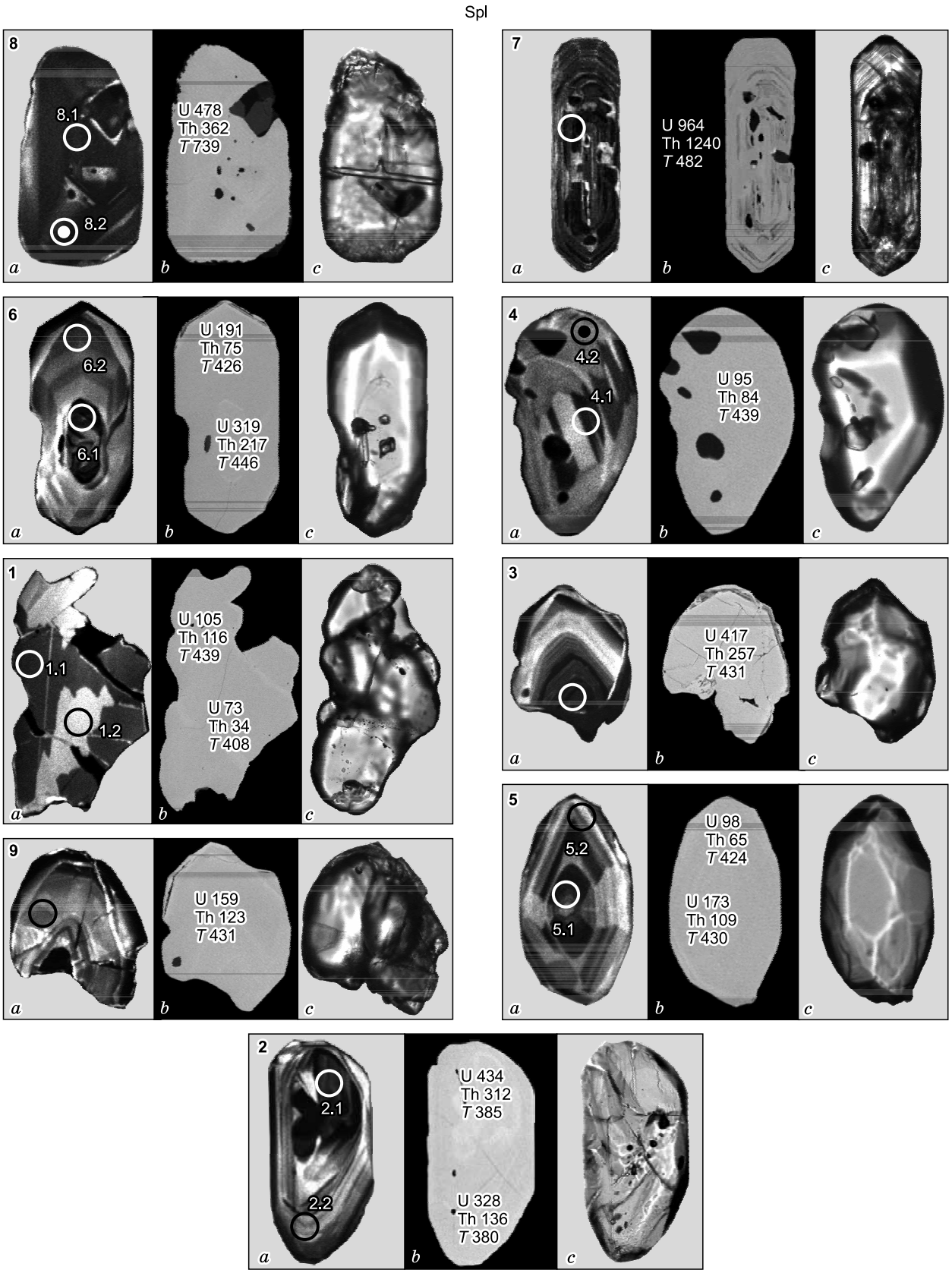

Fig. 2 (*continued*).

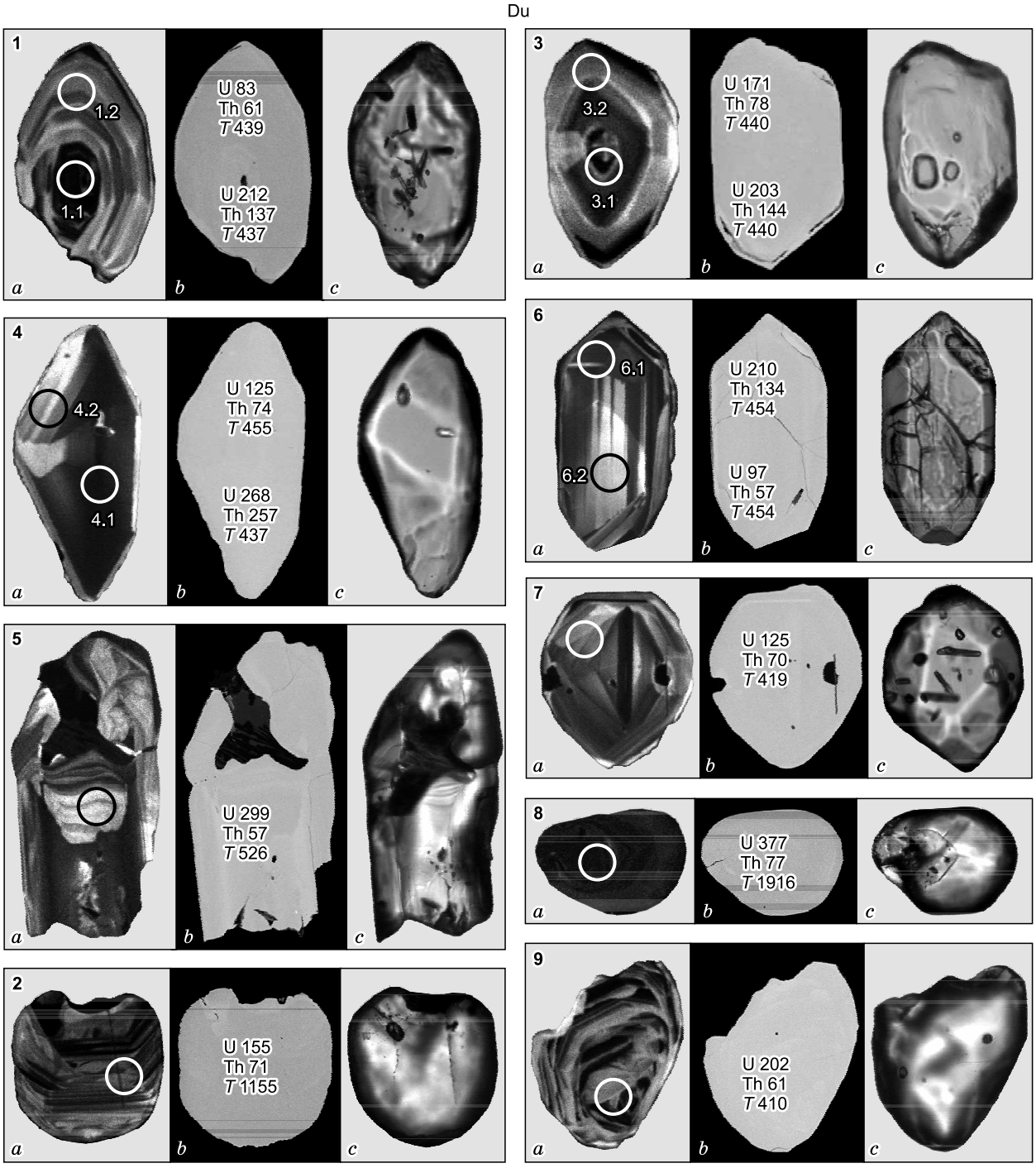

Fig. 2 (*continued*).

ence of dissolved spherical grains (2 and 8), indicative of their sedimentary origin (rounding). However, it can be assumed that these grains have experienced fracturing and dissolution. The preserved part of grain 8 has an embayment, which originally corresponded to the "concave" zone, and is currently partially surrounded by a newly-formed rim. The splintery-looking surface of grain 2 (BSE) and the relief of the negative "defect" are not the result of abrasion. If, however, we take into account the euhedral form of grains 1, 3, 4, 6 and specific grains 7 and 9, and alteration of old grains 2 and 8, the conclusion that dunites contain zircons of different origin seems to be justified.

Zircon age. The similarity in mineralogical and geochemical features of Spl and Pl zircons is also confirmed by isotopic data. They are characterized by significant age heterogeneity (Fig. 3) and coexistence of grains belonging to two different subsets: the main, most representative subset, consisting of grains of similar type and additional subset,

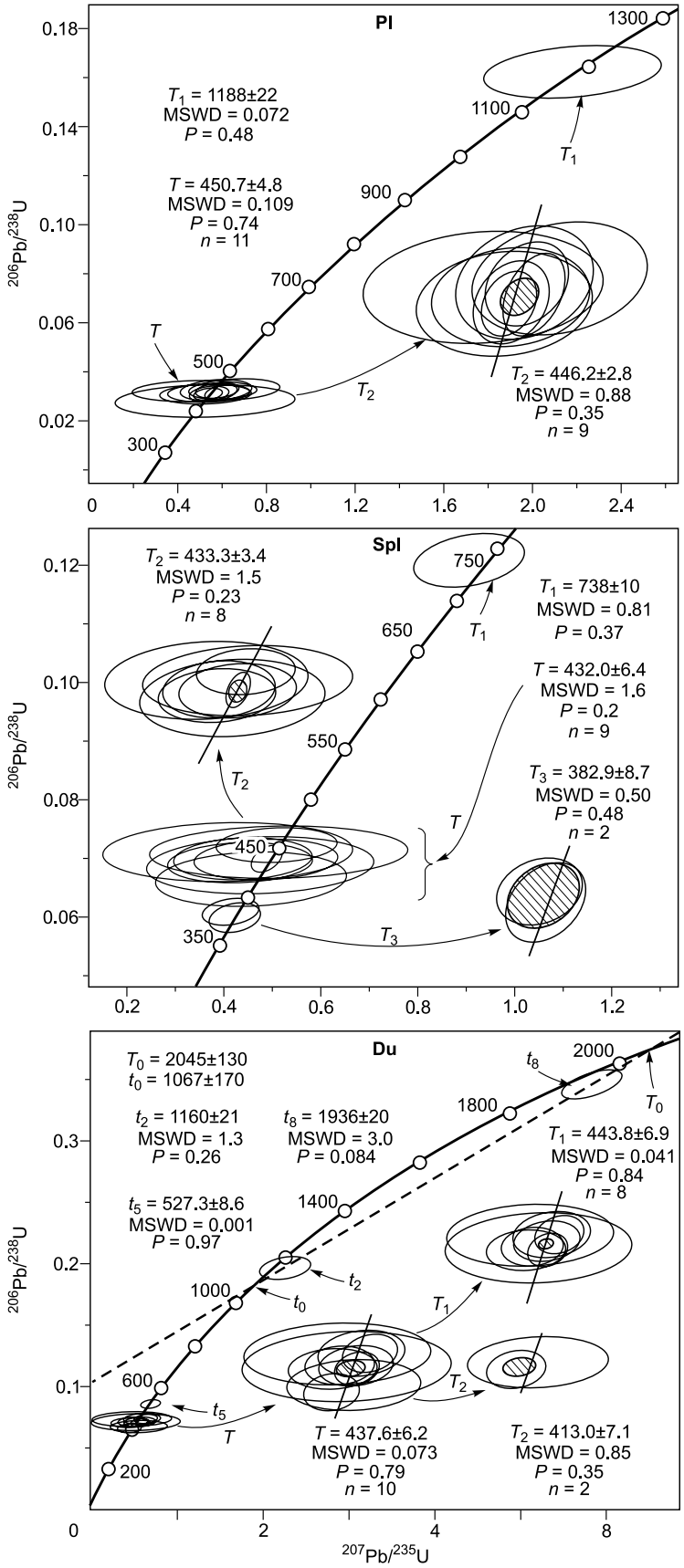

Fig. 3. U–Pb age of zircons from Pl, Spl and Du of the Nurali massif. Pl, T_1, gr. 3; Spl, T_1, gr. 8; Du, t_2, t_5, t_8, gr. 2, 5, 8 (Table 1). *P*, probability.

Table 1. U–Pb age of zircons from plagioclase and spinel lherzolites and dunites of the Nurali massif

Grain and spot	$^{206}Pb_c$,%	Content, ppm		$\frac{^{206}Pb}{^{238}U}$	$\frac{^{232}Th}{^{238}U}$	Age, Ma (1) $\frac{^{206}Pb}{^{238}U}$	*D*, %	Isotope ratios $\frac{^{207}Pb^*}{^{235}U}$	±%	$\frac{^{206}Pb^*}{^{238}U}$	±%	Rho
		U	Th									
Plagioclase lherzolite (K2053, Pl)												
1.1	0.15	855	1001	55.1	1.21	465.4 ± 4.7	–7	0.573	2.4	0.0749	1	0.427
1.2	0.67	173	109	10.8	0.65	451.1 ± 7.9	18	0.580	6.8	0.0725	1.8	0.268
2	0.38	91	35	5.7	0.40	454.0 ± 11.0	73	0.656	13	0.729	2.4	0.190
3.1	1.43	99	27	17.4	0.28	1189.0 ± 22.0	–3	2.180	7.5	0.2025	2.1	0.274
4.1	0.00	147	109	9.0	0.77	446.2 ± 7.8	39	0.598	5	0.0717	1.8	0.362
4.2	0.55	180	70	11.0	0.40	442.8 ± 7.8	–2	0.544	6.7	0.0711	1.8	0.273
5	1.65	155	73	9.7	0.48	445.2 ± 9.2	–7	0.543	14	0.0715	2.1	0.154
6	2.46	48	710	2.9	15.14	425.0 ± 16.0	6	0.530	31	0.0682	4	0.127
7.1	1.86	197	142	12.5	0.75	449.0 ± 10.0	–77	0.480	20.4	0.0722	2.4	0.101
7.2	1.82	162	84	10.0	0.54	442.0 ± 9.8	–17	0.527	16	0.0710	2.3	0.144
8.1	0.35	493	452	30.2	0.95	441.9 ± 6.0	–6	0.539	4.9	0.0709	1.4	0.284
8.2	0.94	145	51	9.1	0.36	452.0 ± 11.0	13	0.576	11	0.0726	2.4	0.214
Spinel lherzolite (K2054, Spl)												
1.1	3.10	105	116	6.6	1.14	439.0 ± 12.0	11	0.550	28	0.0704	2.9	0.102
1.2	2.79	73	34	4.2	0.48	408.0 ± 13.0	–29	0.470	24	0.0653	3.2	0.133
2.1	0.67	434	312	23.1	0.74	385.0 ± 5.7	–29	0.439	6.5	0.0615	1.5	0.236
2.2	0.37	328	136	17.2	0.43	380.3 ± 6.8	–7	0.449	5.8	0.0608	1.8	0.313
3	0.00	417	257	24.8	0.64	431.4 ± 6.3	–13	0.516	3.4	0.0692	1.5	0.437
4.1	4.21	95	84	6.0	0.92	439.0 ± 14.0	–160	0.400	37	0.0705	3.2	0.086
5.1	2.04	173	109	10.5	0.65	430.4 ± 9.5	–13	0.515	17	0.0690	2.3	0.135
5.2	3.57	98	65	0.69	5.96	424.0 ± 13.0	–25	0.490	28	0.0680	3.3	0.119
6.1	1.14	319	217	19.9	0.70	446.9 ± 8.0	–8	0.544	13	0.0718	1.8	0.140
6.2	2.53	191	75	11.5	0.41	426.6 ± 9.3	–94	0.439	20	0.0684	2.3	0.114
7	20.71	964	1240	82.0	1.33	482.2 ± 9.0	179	0.930	14	0.0777	1.9	0.138
8.1	0.82	478	362	50.3	0.78	739.0 ± 11.0	–13	1.021	5.5	0.1214	1.5	0.282
9	2.16	159	123	9.7	0.80	431.5 ± 9.8	–93	0.445	19	0.0692	2.4	0.127
Dunite (K2056, Du)												
1.1	2.50	212	137	13.1	0.67	437.0 ± 9.3	–103	0.443	20	0.0701	2.2	0.110
1.2	3.99	83	61	5.25	0.75	439.0 ± 16.0	–32	0.510	42	0.0705	3.8	0.092
2	0.82	155	71	26.4	0.47	1155.0 ± 21.0	10	2.250	5.4	0.1963	2.0	0.364
3.1	2.00	203	144	12.6	0.73	440.9 ± 9.0	–67	0.477	15	0.0708	2.1	0.145
3.2	0.75	171	78	10.5	0.47	440.5 ± 9.2	12	0.557	14	0.0707	2.2	0.159
4.1	0.60	268	257	16.3	0.99	437.4 ± 7.7	20	0.560	8	0.0702	1.8	0.229
4.2	1.28	125	74	7.93	0.61	455.0 ± 11.0	18	0.586	15	0.0731	2.4	0.163
5	0.86	299	57	22	0.20	526.6 ± 8.6	1	0.681	6.7	0.0851	1.7	0.253
6.1	1.20	210	134	13.3	0.66	454.7 ± 8.9	50	0.627	8.9	0.0731	2.0	0.228
6.2	3.76	97	57	6.31	0.61	454.0 ± 14.4	–94	0.470	40	0.0729	3.2	0.080
7	3.28	125	70	7.45	0.58	419.0 ± 12.0	34	0.540	25	0.0671	2.9	0.117
8	0.45	377	77	113	0.21	1916.0 ± 23.0	4	5.840	2.5	0.3461	1.4	0.567
9	1.49	202	61	11.6	0.31	410.9 ± 8.6	–72	0.438	13	0.0658	2.2	0.168

Note. All errors are presented at ±1σ. Pb_c and Pb*, common and radiogenic lead. Error in standard calibration is 0.65%. (1), corrected for ^{204}Pb. *D,* discordance. Rho, $^{207}Pb^*/^{235}U$–$^{206}Pb^*/^{238}U$ error correlation coefficient. Data reduction was carried out using the ISOPLOT/EX software (Ludwig, 2001).

consisting of a few grains with varied characteristics. Grain 3 (Pl, Table 1) is characterized by lower Th and Th/U values and the oldest age (T_1 = 1188 ± 22 Ma). Grain 8 (Spl) is also older (T_1 = 738 ± 10 Ma) than the remaining grains. They represent relics of older grains.

The analytical data show that the age of Pl zircon grains belonging to the main subset is T = 450.7 ± 4.8 Ma. If we do not take into account grains 1.1 and 6 (Table 1), which are characterized by higher Th and Th/U values, and "extreme" values of $^{206}Pb/^{238}U$ ages (465, 425 Ma), the remaining grains form a tight cluster yielding the most reliable concordant age of T_2= 446.2 ± 2.8 Ma.

Under the influence of "metamorphism" associated with the formation of vein bodies and "young" zircons (T_3 = 382.9 ± 8.7 Ma), the age of the main subset of Spl zircon grains (Figs. 2 and 3) became younger (T_2 = 433.3 ± 3.4 Ma). This is confirmed by older ages of some preserved Spl zircon grains (6.1, 446.9 ± 8 Ma, Table 1). Altogether, these data for zircons of the main type suggest a subsynchronous crystallization in Spl and Pl.

Du zircons typically have wide intergrain variations in age. Zircons comparable to the main subset of grains from lherzolites yielded an integrated age of T = 437.6 ± 6.2 Ma. Grains 7 and 9 with specific internal structures (Fig. 3) are characterized by the youngest age (T_2 = 413.0 ± 7.1 Ma). If we exclude them from the main subset, the remaining grains yielded a concordant age of T_1 = 443.8 ± 6.9 Ma, which corresponds most closely to the age of dunites. This may indicate some local event, which produced grain 5 with a concordant age of T_5 = 527.3 ± 8.6 Ma. The ages of relict grains 2 and 8 calculated using the $^{207}Pb/^{235}U$ ratio are T_2 = 1160 ± 21 Ma and T_8 = 1936 ± 20 Ma. These dates represent a rejuvenation age, not a crystallization age. By combining grains 2 and 8, which yielded similar right-hand shifts of data points relative to concordia, we can calculate the possible youngest age of the dunite T_0 = 2045 ± 130 Ma.

U and Th geochemistry of zircons. Zircons from lherzolite and dunite show a direct correlation between their U and Th contents (Fig. 4), which tend to decrease in the late generations of grains (tr. I). The similarity in these trends suggests that they belong to a single geochemical space, i.e. derivation of zircons from the same source. Zircons from dunite, especially early generation grains (Fig. 4,*A* and *B*), show little variation in their U and Th content compared to zircons from lherzolite, but they are characterized by the maximum diversity. The oldest grains (2, 5, and 8) and grains with an anomalous structure (7 and 9) form an isolated cluster B, with the smallest variation in Th and significant variation in U.

Comparison of U contents and $^{206}Pb/^{238}U$ ages (Table 1, Fig. 2) shows that Spl zircons have experienced a more progressive rejuvenation than Pl zircons, which is associated not only with the growth of young crystals (2.1–2.2), but also with the effects of intense deformation in Spl lherzolites.

Rare-earth elements in zircons. The REE patterns for zircons (Table 2, Fig. 5) are characterized by HREE enrichment and the presence of positive Ce and negative Eu anomalies. These features are indicative of their magmatic origin (Hoskin, 2005; Fedotova et al., 2008; Balashov and Skublov, 2011; Krasnobaev et al., 2011; Skublov et al., 2012).

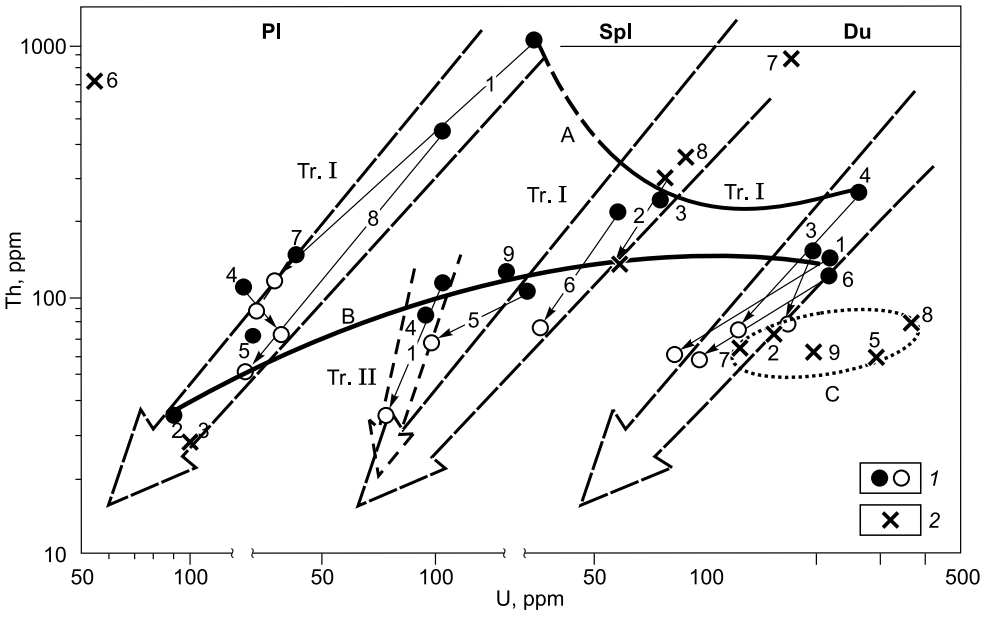

Fig. 4. U and Th in zircons from Pl, Spl and Du of the Nurali massif. *1*, early (filled circle), late (empty circle), (connected with arrows) generations of zircons grains belonging to the main subset; *2*, isolated additional grains. Tr. I, evolutionary trends of zircons from lherzolites and dunites. Curves A and B limit variations in the early generations of zircons from the main subset. Tr. II shows the boundaries of the evolution of zircons from Spl (4, 1.1–1.2, 5.2), which differ from grains from the main subset. Area C (Du) depicts zircons with specific features (2, 5, 7, 8, 9), which are preserved in dunites.

Table 2. REE contents (ppm) of zircons from plagioclase (K2053) and spinel lherzolites (K2054) and dunites (K2056) of the Nurali massif

Component	Sample K2053								Sample K2054					
	1.1	1.2	3.1	3.2	4.1	4.2	8.1	8.2	9.1	9.2	1.1	1.2	2.1	2.2
La	1.17	0.28	1.18	0.12	0.44	0.31	0.21	0.31	35.42	1.92	0.13	0.11	0.16	0.18
Ce	131.90	26.00	15.40	4.30	32.10	20.30	99.00	20.20	264.30	10.03	28.50	18.60	38.10	28.80
Pr	1.67	0.26	1.44	0.07	0.24	0.25	0.32	0.31	29.09	1.62	0.33	0.17	0.25	0.23
Nd	15.10	1.83	8.36	1.05	2.26	2.01	3.39	1.89	176.24	13.72	5.34	1.99	2.70	1.74
Sm	20.18	2.26	9.87	2.56	3.93	2.48	6.13	1.87	55.80	4.29	9.50	2.87	4.18	2.00
Eu	6.33	0.61	0.94	0.21	1.35	0.89	1.86	0.84	21.59	0.70	2.13	0.69	1.48	0.66
Gd	67.73	9.87	39.43	15.06	19.04	10.55	32.96	6.56	79.07	5.56	34.32	11.84	18.90	7.83
Dy	179.90	38.80	136.10	57.10	74.30	50.50	129.80	26.60	149.30	9.07	88.00	38.90	72.30	31.70
Er	404.30	113.20	248.60	131.10	196.60	163.50	307.00	74.80	399.10	31.51	160.80	82.80	179.50	82.10
Yb	850.80	310.80	394.70	217.00	487.40	436.40	643.10	202.50	1087.40	126.65	288.60	176.30	430.40	207.40
Lu	139.70	60.00	61.60	35.80	95.70	90.90	112.00	38.20	220.80	32.18	50.70	30.40	82.80	42.00
Total	1818.85	563.86	917.74	464.49	913.37	778.09	1335.85	374.02	2518.10	237.28	668.33	364.72	830.75	404.63
SI/SII	3.23		1.98		1.17		3.57		10.61		1.83		2.05	
$(Sm/La)_N$	27.50	13.10	13.40	34.11	14.12	12.98	47.77	9.47	2.52	3.57	114.95	42.33	40.94	17.38
$(Yb/La)_N$	1067.30	1663.90	493.97	2658.00	1609.20	2103.80	4606.20	944.23	45.18	96.87	3210.74	2389.72	3873.20	1653.70
Ce/Ce*	22.80	23.64	2.87	11.32	23.45	17.62	92.90	15.56	1.99	1.37	32.83	33.29	45.54	34.07
Eu/Eu*	0.52	0.39	0.15	0.10	0.48	0.53	0.40	0.73	0.99	0.44	0.36	0.36	0.51	0.51

Component	Sample K2054						Sample K2056						
	4.1	4.2	6.1	6.2	8.1	8.2	3.1	3.2	5	6.1	6.2	8	2
La	0.14	0.08	37.16	4.62	17.91	1.19	22.35	0.12	0.06	5.99	0.05	0.189	0.07
Ce	46.50	13.90	409.30	61.10	84.60	17.75	290.50	28.40	16.60	69.90	9.00	4.60	52.40
Pr	0.28	0.08	42.19	2.39	5.07	0.52	8.34	0.16	0.02	4.38	0.05	0.09	0.09
Nd	3.94	0.91	272.24	13.56	25.59	5.73	27.72	1.78	0.15	23.05	0.98	0.95	0.90
Sm	6.46	1.50	156.78	4.73	12.60	7.82	6.31	3.57	1.31	11.84	2.33	2.98	2.20
Eu	2.52	0.59	26.90	1.08	1.48	0.81	1.53	1.34	1.03	2.31	0.63	0.29	0.25
Gd	35.60	7.47	169.45	17.18	51.68	37.82	7.86	20.35	6.93	19.44	13.98	17.28	14.02
Dy	140.10	33.10	159.10	64.00	170.10	151.02	27.70	90.00	8.80	58.20	62.60	51.70	70.60
Er	361.50	99.80	204.00	181.00	358.50	310.24	69.80	268.30	29.40	151.00	172.70	118.40	186.10
Yb	810.80	279.00	448.50	439.90	613.20	512.17	200.20	688.40	87.00	398.30	407.30	270.80	401.10
Lu	154.80	55.60	84.20	85.10	98.70	80.64	46.60	137.00	19.20	79.00	77.50	45.80	67.40
Total	1562.64	492.07	2009.92	874.63	1439.33	1125.74	708.95	1239.48	162.86	823.33	747.16	513.16	795.12
SI/SII	3.18		2.30		1.26		0.57			1.10			
$(Sm/La)_N$	73.56	28.44	6.75	1.64	1.13	10.48	0.451	48.12	35.40	3.16	67.74	25.27	51.26
$(Yb/La)_N$	8484.84	4860.80	17.76	140.17	50.39	630.52	13.18	8519.52	2193.85	97.84	10890.77	2110.10	8582.78
Ce/Ce*	57.03	39.87	2.50	4.45	2.14	5.43	5.14	49.65	107.96	3.30	42.85	8.72	159.32
Eu/Eu*	0.51	0.53	0.50	0.37	0.17	0.14	0.66	0.49	0.13	0.46	0.33	0.12	0.14

Note. SI/SII, total REE in early—late generations of heterogeneous grains. $(Sm/La)_N$, $(Yb/La)_N$, Ce/Ce*, Eu/Eu* were normalized to chondrite values (McDonough and Sun, 1995). $Ce/Ce^* = Ce/(La \times Pr)^{1/2}$; $Eu/Eu^* = Eu/(Sm \times Gd)^{1/2}$.

The REE patterns for most early and late generation zircons from Pl (Fig. 5) are characterized by the presence of Ce and Eu anomalies and HREE > LREE. The successive generations of grains 1, 3, and 4 are characterized by similar REE patterns, suggesting their derivation from the same source, which shows changes in the composition during fractional crystallization. The situation with grain 9 is different: both generations of this grain show a formal similarity in their REE patterns but a flatter LREE profile, indicative of a metasomatic origin. The pronounced evolutionary trend in the REE patterns reflects the tendency toward the magmatic (M) origin of grain 3, and hydrothermal (H) (or metasomatic in this case) origin of grain 8 (Fig. 6). It is noteworthy that variation of LREE depletion is observed in coexisting crystals, i.e., no averaging of their REE content took place. Therefore, the absence of such averaging makes zircon a

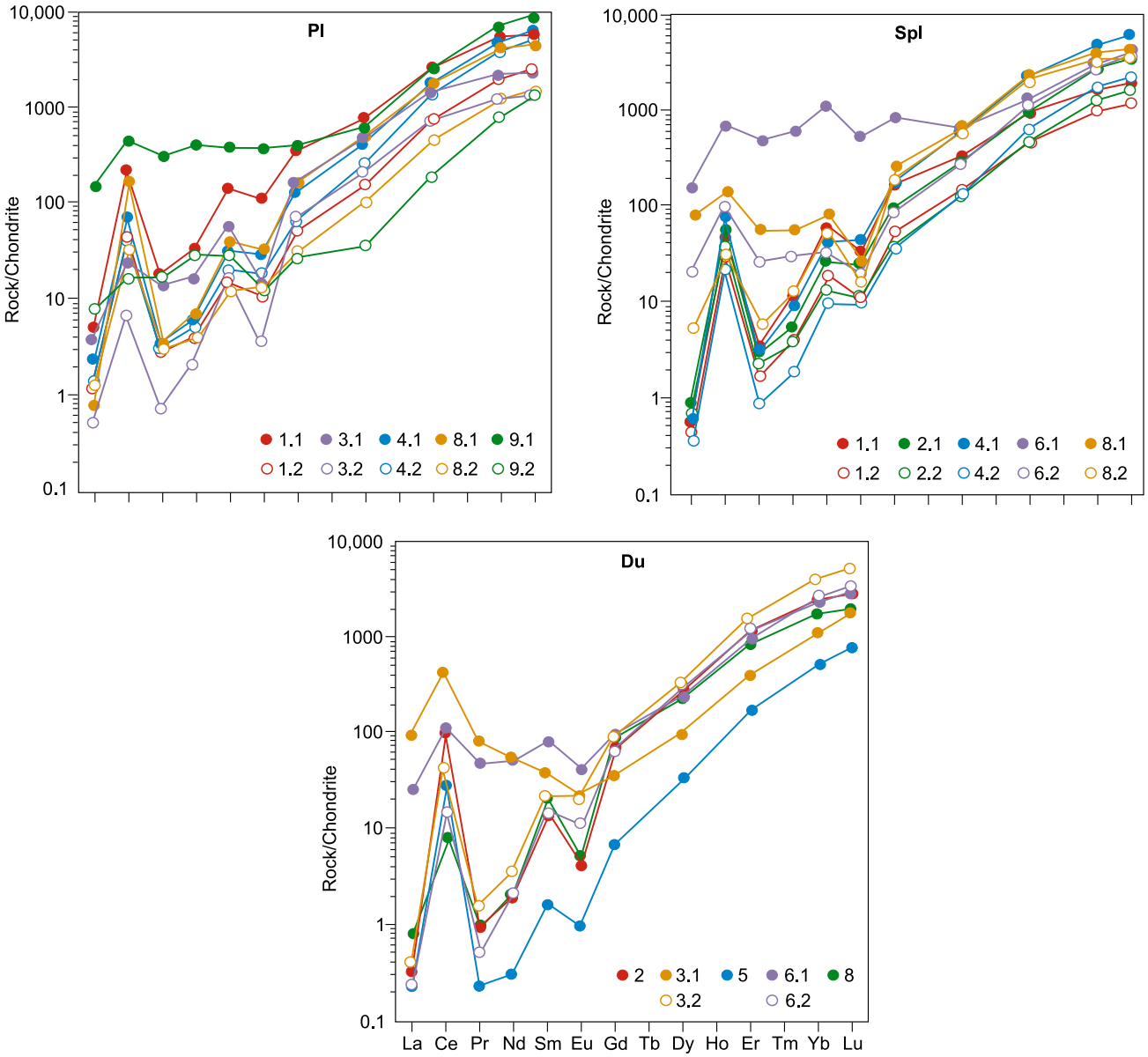

Fig. 5. REE patterns for zircons from Pl, Spl, and Du of the Nurali massif. Data on zircons were collected at the points (Fig. 2) that were previously analyzed for U–Pb age. The numbers of grains are the same as in Fig. 2, grain 9 from Pl was measured only for REE. Early generations are depicted by filled circles, late generations are depicted by empty circles.

unique and the most powerful geochronometer for ultramafic rocks. This is the advantage of the zircon matrix, whose main properties include robustness, stability, genetic sensitivity, the ability to retain information on the timing of its evolutionary growth.

The REE patterns for different generations of zircon grains 1, 2, 4 from Spl (Fig. 5) largely resemble those of zircon grains 1, 3, 4 from Pl, which also suggests their magmatic origin. The REE patterns for both early and late generations of grains 6 and 8 are different, pointing to their different origin. In addition, the REE patterns for the early generations of these grains show either certain (6.1) or a close (8.1) resemblance to the REE patterns of metasomatic zircons. The REE patterns of late generation grain 8 are broadly similar to that of magmatic zircons, but actually represent secondary generation zircons, which have experienced recrystallization.

Many Du zircons differ considerably from zircons from lherzolite. First of all, this is true for older grains 2, 5, and 8, and in which the values of Ce and Eu anomalies and HREE contents suggest their probable origin by the magmatic processes (Fig. 6). For grain 3, the REE patterns for the early generation and late generation (3.2) correspond to metasomatic and magmatic zircons, respectively. The situation

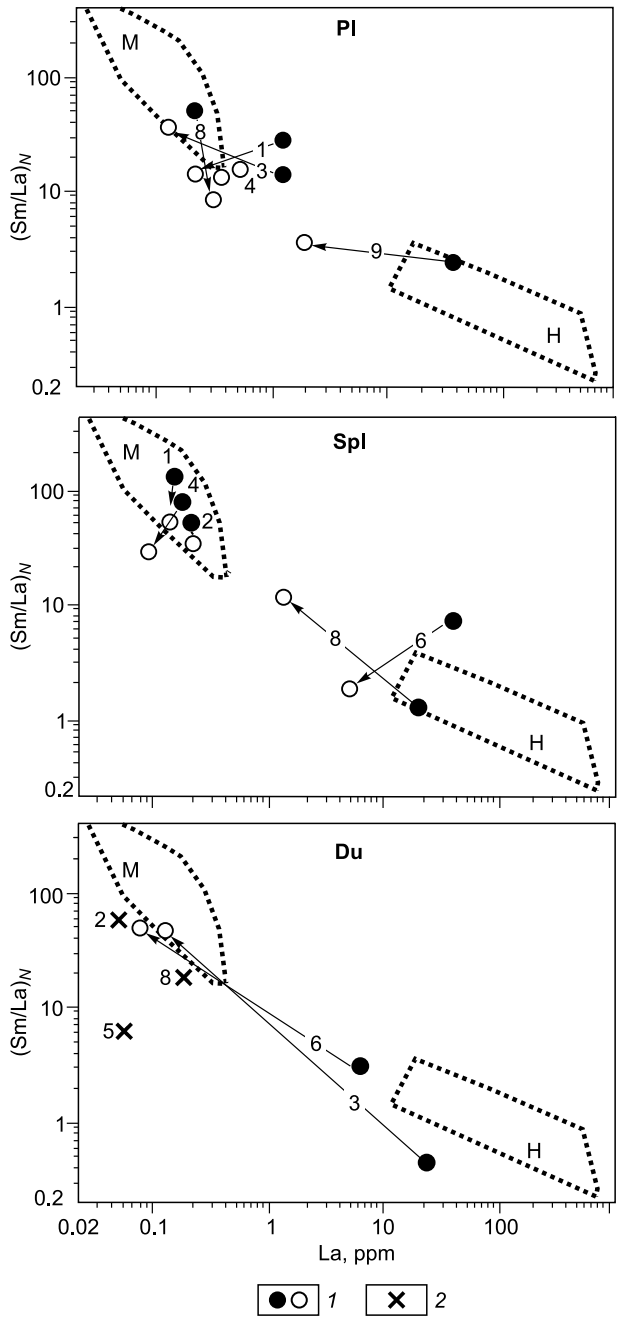

Fig. 6. Genetic classification of zircons from Pl, Spl and Du of the Nurali massif, after Hoskin (2005). M and H, fields of magmatic and hydrothermal (metamorphic, altered) zircon types. All elements were normalized to chondrite values (McDonough and Sun, 1995). *1*, zircons of the main subset, early generations (filled circle)—late generations (empty circle) are connected by arrows; *2*, isolated grains of a different origin.

with grain 6 is more complicated: the early generation of this grain is of metasomatic origin, while late generation is of magmatic or, more precisely, pseudo-magmatic origin. This zircon paradox (for dunites), when zircons of the second generation acquire the properties of igneous (pseudo-primary) zircons, has no logical explanation yet. The final conclusion requires the more representative datasets.

The above problems can be adequately solved using fragments of REE patterns for zircons in the La–Sm/La and Sm/La vs. Ce/Ce* diagrams (Fig. 6) (Hoskin and Schaltegger, 2003; Hoskin, 2005). First of all, the NM ultramafic rocks are clearly dominated by magmatic or similar type zircons belonging to the main subset. The second important conclusion is that zircons from Spl are more "magmatic" compared to zircons from Pl, because the data points of the latter have a slight shift toward the H-type zircons. It should be noted that this situation is supported by petrological evidence. It was shown that plagioclase lherzolite is usually formed after spinel lherzolite, which is weakly deformed and has a protogranular texture, whereas the plagioclase lherzolite typically shows strain features, such as porphyroclastic and cataclastic fabrics (Chashchukhin et al., 2007).

The REE spectra of the old grains (8, Spl; 9, Pl) fall directly into the H-type zircon field, which received increased α-radiation doses, resulting in the transition to the metamict state. Changes in the growth environment and the development of conditions favorable for the formation of zircons belonging to the main subset resulted in an increase in their crystallinity and shift toward the M-type zircon field.

The assignment of the early generations of Du zircons to the H-type could not be given any logical explanation (Dobretsov et al., 2019). However, the transition of their second generations to the field of the main subset of zircon grains seems to be quite logical and is confirmed by similar ages of the early–late generations.

CONCLUSIONS

1. Most zircons of the main subset belong to magmatic type, which is characterized by free crystallization in melts, corresponding to the 4π symmetry.

2. The age of zircons from lherzolites belonging to the main subset falls within the interval 433–446 Ma (T_{mean} = 439 ± 4 Ma) and is close to their crystallization age. The most reliable age of zircons from dunite is 443.8 ± 6.9 Ma. Altogether, both ages suggest a subsynchronous crystallization in lherzolite and dunite and, correspondingly, can be interpreted as the age of formation of the Nurali massif (S_1). The metamorphic processes within the massif are characterized by a concordant zircon age of 413.0 ± 7.1 Ma. The final stage of the evolution of the massif was accompanied by the formation of "young" metasomatic zircons with an age of 320–385 Ma (D_3).

3. The Precambrian ages (1190, 2045 Ma) reflect the multiscale stages of transformation of relic zircons inherited from mantle-derived ultramafic rocks with ages of 2000 Ma. The evolution of ultramafic rocks was accompanied by local melting processes, as indicated by the presence of melt inclusions in zircons with a concordant age of 527.3 ± 8.6 Ma (gr. 5, DU).

REFERENCES

Balashov, Yu.A., Skublov, S.G., 2011. Contrasting geochemistry of magmatic and secondary zircons. Geochem. Int. 49 (6), 594–604.

Chashchukhin, I.S., Votyakov, S.L., Shchapova, Yu.V., 2007. Crystal Chemistry of Spinel and Oxytermobarometry of Ultramafites of Folded Regions [in Russian]. IGG, UrO RAN.

Dobretsov, N.L., Chepurov, A.I., Sonin, V.M., Zhimulev, E.I., 2019. Stability of zircon in the system $MgO–SiO_2–H_2O$ at 2.5 GPa. Russian Geology and Geophysics (Geologiya i Geofizika) 60 (4), 447–450 (527–531).

Fedotova, A.A., Bibikova, E.V., Simakin, S.G., 2008. Ion-microprobe zircon geochemistry as an indicator of mineral genesis during geochronological studies. Geochem. Int. 46 (9), 912–927.

Fershtater, G.B., 2013. Paleozoic Intrusive Magmatism of the Middle and Southern Urals [in Russian]. IGG, UrO RAN.

Fershtater, G.B., Bea, F., 1996. Geochemical typification of the Ural Ophiolites. Geochimiya, No. 3, 195–218.

Fershtater, G.B., Kotov, V.B., Smirnov, S.V., Pushkarev, E.V., Salnikov, E.B., Kovach, V.P., Yakovleva, S.Z., Berezhnaya, N.G., 2000. U–Pb zircon age of diorite from the Nurali lherzolite-gabbro massif in the Southern Urals. Dokl. Earth Sci. 371 (1), 96–100.

Hoskin, P.W., 2005. Trace-element composition of hydrothermal zircon and the altetation of Hadean zircon from the Jack Hills, Australia. Geochim. Geosmochim. Acta 69 (3), 637–648.

Hoskin, P.W., Schaltegger, O., 2003. The composition of zircon and Igneous and metamorphic petrogenesis of zircon. Rev. Mineral. Geochem. 53 (3), 27–62.

Knipper, A.L., Sharaskin, A.Y., Savelieva, G.N., 2001. Geodynamic settings of the formation of different types of ophiolite sections. Geotektonika, No. 4, 3–21.

Krasnobaev, A.A., Rusin, A.I., Rusin, I.A., Busharina, S.V., 2011. Zircons, zircon geochronology, and petrogenetic problems of the lherzolite massifs of the South Urals. Geochem. Int. 49 (5), 482–497.

Ludwig, K.R., 2001. Users Manual for Isoplot/Ex rev. 2.49. Berkeley Geochronol. Center Spec. Publ. 1a.

McDonough, W.F., Sun S.-s., 1995. The composition of the Earth. Chem. Geol. 120 (3–4), 223–253.

Pertsev, A.N., Spadea, P., Savelieva, G.N., Gareggo, L., 1997. Nature of the transition zone in the Nurali ophiolite, southern Urals. Tectonophysics 276 (1–4), 163–180.

Popov, V.S., Kremenetskii, A.A., Belyatskii, B.V., 2008. Pre-Ordovician Sm–Nd isotopic age of ultramafic rocks in the ophiolitic belts of the Urals (specified data), in: Structural and Compositional Complexes and Problems of Geodynamics in the Precambrian [in Russian]. IGG UrO RAN, Yekaterinburg, pp. 100–103.

Puchkov, V.N., 2010. Geology of the Urals and Cisuralian Area (Current Issues of Stratigraphy, Tectonics, Geodynamics and Metallogeny) [in Russian]. IG UNTs RAN, Ufa.

Rudnik, G.B., 1965. Petrogenesis of Ultramafic Rocks of the Nurali Massif in the Southern Urals, in: The Relationship between Magmatism and Metamorphism in the Genesis of Ultramafic Rocks [in Russian]. Nauka, Moscow, pp. 68–101.

Savelieva, G.N., 1987. The Gabbro-Ultramafic Complexes of the Uralian Ophiolites and Their Analogues in the Modern Oceanic Crust [in Russian]. Nauka, Moscow.

Savelieva, G.N., 2011. Ophiolites in European Variscides and Uralides: Geodynamic setting and metamorphism. Geotectonics 45 (6), 439–452.

Savelieva, G.N., Denisova, E.A., 1983. The structure and petrology of the ultramafic Nurali massif in the South Urals. Geotektonika, No. 2, 42–57.

Skublov, S.G., Berezin, A.V., Berezhnaya, N.G., 2012. General relations in the trace-element composition of zircons from eclogites with implications for the age of eclogites in the Belomorian mobile belt. Petrology 20 (5), 427–449.

Tessalina, S.G., Bourdon, B., Gannoum, A., Campas, F., Birck, J.L., Allegre, C.J., 2007. Complex Proterozoic to Paleozoic history of the upper mantle recorded in the Urals lherzolites massifs by Re–Os and Sm–Nd systematics. Chem. Geol. 240 (1–2), 61–84.

Williams, I.S., 1998. U–Th–Pb geochronology by ion microprobe, in: McKibbe, M.A., Shanks, W.C., Ridley, W.I. (Eds.), Applications of Microanalytical Techniques to Understanding Mineralizing Processes. Rev. Econ. Geol., Vol. 7, pp. 1–35.

Editorial responsibility: N.L. Dobretsov